PHYSICAL REVIEW A **73**, 021802(R) (2006)

Scanning interferometric microscopy for the detection of ultrasmall phase shifts in condensed matter

J. Hwang,[1,2] M. M. Fejer,[1] and W. E. Moerner[2]
[1]*Department of Applied Physics, Stanford University, Stanford, California 94305, USA*
[2]*Department of Chemistry, Stanford University, Stanford, California 94305, USA*
(Received 14 April 2005; published 17 February 2006)

We describe a scanning optical microscope based on polarization Sagnac interferometry for measuring ultrasmall phase shifts, and use this method to detect small numbers of absorbing molecules in a solid without the use of fluorescence. The absorption and concomitant optical phase shift of terrylene dopant molecules in a *p*-terphenyl host crystal are made time dependent by periodic optical saturation of the sample. A detection sensitivity of 8.75×10^{-8} rad is achieved with a 0.078 Hz bandwidth, and detection of signals from as few as 19 ± 3 terrylene molecules is demonstrated at room temperature.

DOI: 10.1103/PhysRevA.73.021802 PACS number(s): 42.62.Fi, 07.60.Ly, 39.30.+w, 82.53.Kp

Ultrasensitive optical spectroscopy of condensed phases in fields ranging from physical chemistry [1] to single-molecule biophysics [2] often make use of emission from highly fluorescent molecules such as organic dyes [3,4], or autofluorescent proteins [5]. Although for a number of reasons fluorescence methods are currently widely used in single-molecule studies, sensitive detection of fluorescence in condensed matter also presents several experimental issues, most notably the need to count single photons while rigorously excluding counts from all sources of unwanted fluorescence or Raman scattering from trillions of host molecules. These issues are even more challenging in nonartificial experimental environments such as inside cells or turbid hosts. An alternative detection method is direct measurement of absorption, in which the absorption events are not detected by recording subsequent fluorescence but by the change in the power or phase of a laser beam probing the sample. In this case, any spurious emission from the sample or substrate is not critical, and all the photons in the entire laser beam probing the sample can be used to sense the signal of interest.

Frequency-modulation (FM) spectroscopy [6] was the first method to allow detection of the absorption of single molecules in condensed matter [7]. However, in these liquid helium temperature experiments, the resulting absorption cross sections approached the maximum possible values on the order of the optical wavelength squared ($\sim10^{-10}$ cm^2). Here we concentrate on the important room temperature regime, a considerable challenge because conventional FM spectroscopy fails when absorption lines are broad; moreover phonon broadening leads to peak absorption cross sections which are $\sim10^5$ times smaller than at cryogenic temperatures. An existing direct absorption method is cavity ring-down spectroscopy (CRDS) [8], which exploits multipass enhancement and perturbations of cavity lifetime in a Fabry-Perot interferometer. While impressive sensitivities have been obtained in uniform samples, scanning microscope configurations are yet to be developed. In bulk liquid and thin film solid CRDS studies, 2×10^{-7} sensitivity with 1 s averaging time [9] and 1.3×10^{-7} with roughly 6 ms averaging time [10] were achieved, respectively, among other attempts [11,12]. In the former example, the sensitivity corresponds to detecting roughly 10^8 molecules in the 0.5 μl probed volume. In this paper, we suggest and demonstrate a new type of absorption spectroscopy implemented as a scanning optical microscope capable of ultrasensitive measurements of molecules in condensed matter samples at room temperature. This method, although a single-pass measurement, achieves detection sensitivity of a few absorbing molecules.

Here we choose to measure the phase shift of a probe beam induced by the molecular absorption events rather than the change in transmission of the beam because higher probing power can be used without saturation effects. As is well known, in optically thin samples there is a fundamental connection between absorption and dispersion described by the Kramers-Kronig (KK) relations [13]. For the strongly allowed lowest electronic transition of the highly photostable system of terrylene in a *p*-terphenyl host crystal [14–16], the phase shift per molecule at 633 nm is $\sim4.1\times10^{-9}$ rad per μm^2 of the probe beam area.

Out of the several interferometers designed for sensitive detection of phase shifts, the Sagnac interferometer [17] has certain advantages in this application, notably that the clockwise (CW) and counterclockwise (CCW) beams follow exactly the same path inside the interferometer loop (see Fig. 1). The resulting common mode rejection provides robust elimination of fringe shifts due to technical effects such as phase noise of the probing laser, as well as mechanically or thermally induced path-length changes that occur over times longer than the round-trip time in the loop. No locking is necessary, a technological advantage over other interferometers such as the Michelson or Mach-Zehnder. As a result, Sagnac interferometers have been used for sensing nonreciprocal phase shifts in fiber optic gyroscopes [18] and Faraday-effect current sensors [19]. The Sagnac interferometer is sensitive to reciprocal path length changes that occur faster than the round-trip time of the loop, as has been proposed for gravitational wave detectors [20], and demonstrated in various time-gated devices in fiber-optic signal processing [21–24]. Here, we use a Sagnac interferometer to read out the fast changes in phase shift due to pulsed saturation of a molecular sample to implement a scanning microscope.

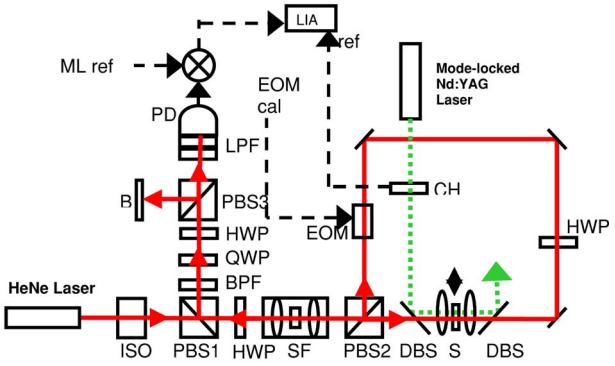

FIG. 1. (Color online) Schematic for optical setup and signal processing electronics. ISO, Faraday isolator; BPF, band pass filter; LPF, long-pass filter; QWP, quarter-wave plate; CH, chopper; PD, photodiode; B, beam block; ML ref, mode-locker reference signal; EOM cal, calibrated driving voltage for electro optic modulator. All the other symbols and details are explained in the text.

In order to generate a time-dependent phase shift from the molecular sample (S), we modulate the refractive index of the sample by pumping the molecule into its excited state in a repetitive fashion using a frequency-doubled mode-locked Nd:YAG laser [82 MHz repetition rate, pulse width ~ 100 ps $\ll T_1$), injected into the loop using dichroic beam splitters (DBS) and focused into and out of the sample by two objective lenses]. After a molecule in the sample is excited, for a time of order T_1 (=3.8 ns) the dispersive phase-shift spectrum of the molecule is inverted compared to that of a molecule in the ground state. A sample positioned a distance L_S from the center of the loop is interrogated by the CW and CCW beams at times separated by $t_S = 2L_S/c$, so that as long as $t_S > \sim T_1$, the CW and CCW beams will see equal and opposite phase shifts over a time interval of approximately T_1 [18]. To maximize the response, the loop length is set to match the repetition period of the pump laser, and the phase shift from the sample results in an ac signal of frequency $f = 1/t_S$ in the detection port, in a manner we now describe.

Of the several possible Sagnac configurations, we use here the polarization Sagnac design [25] proposed earlier for future gravitational-wave detectors [26–29]. Referring to Fig. 1, the 633 nm linearly polarized probe beam passes through an isolator and a polarizing beam splitter (PBS1), is rotated to 45° by a half-wave plate (HWP), and is spatially filtered (SF) before reaching PBS2, thus generating two counterpropagating beams around the Sagnac loop. The HWP in the interferometer loop rotates the plane of polarization by 90°, ensuring that there is only one polarization at any given point around the loop. If there are differential phase shifts between the CW and CCW beams, the originally linearly polarized probe beam leaves the same port of the interferometer elliptically polarized. The minor axis of the ellipse is equivalent to the dark fringe of the interferometer, whose amplitude in the small-signal limit is proportional to the phase difference between the two counterpropagating beams. The outgoing probe beam travels back through the first HWP, and upon encountering PBS1, only the component of the field along the minor axis of the ellipse is reflected toward the detection port, which therefore ideally has zero background. A local oscillator that serves the useful purpose of linearizing the dependence of the detected signal on the phase-shift difference is derived from a small fraction of the bright port (i.e., major axis of the ellipse) field that leaks toward the detector through the intentionally imperfect PBS1. This field, with power P_{LO}, is orthogonal in polarization and is path length matched to the dark port signal. Introducing another quarter-wave plate (QWP) in the detection port linearizes the response by mixing the local oscillator and dark port fields. We implement this design as a scanning microscope by mounting the sample on a two-dimensional (2D) scanner.

The signal-to-noise ratio of this interferometric scanning microscope can be derived following the analyses in Refs. [16,27,30]. Using the criterion of signal-to-noise ratio $(SNR) = 1$ to calculate the shot-noise-limited minimum detectable phase shift, $\delta\phi$ [i.e., the peak magnitude of the time-varying sample phase shift $\delta\phi(t)$], normalized by the square root of detection bandwidth B is

$$\frac{\delta\phi}{\sqrt{B}} = \sqrt{\frac{h\nu(P_{dp} + P_{LO} + P^*)}{\eta\eta_t P_{LO} P_{in} C^2}}, \tag{1}$$

with h Planck's constant and ν the optical frequency. P_{in} is the input probe laser power entering the interferometer, η_t is the power transmission factor reduced from unity by losses in the interferometer optics, and η is the quantum efficiency of the photodiode. The contrast ratio C is defined for this specific configuration as

$$C \equiv \frac{P_{bp} - P_{dp}}{P_{bp} + P_{dp}} = \cos\Delta\phi \cong \cos\phi_0,$$

where P_{dp} (P_{bp}) is the dark (bright) port [minor (major) axis of the ellipse] power. The spatial filter plays a key role in maintaining single-mode character of the beam; in the ideal case of perfect overlap, P_{dp} would arise only from the (very small) sample modulation contribution, so C would be close to unity. In a practical system, C is not unity and is given by the cosine of nonideal static phase difference ϕ_0 [total phase difference is $\Delta\phi = \phi_0 + \delta\phi(t)$]. P^* is the additional dc power at the detector due to the leaky beam splitter and imperfect contrast ratio.

From Eq. (1), an obvious way to increase sensitivity is to increase P_{in}, but only up to the limit set by the saturation intensity of the molecular sample. The 633 nm probe-laser power at the sample is roughly 8 mW, while the saturation power is estimated to be 30 mW for terrylene in p-terphenyl (cross-section estimated as 4×10^{-17} cm^{-2} at 633 nm) with a 1.7 μm^2 probe spot size [15,30]. It is important to note that while the optical power the photodiode has to tolerate is only $P_{LO} + P_{dp} + P^*$, the SNR improves as the square root of the full power entering the interferometer P_{in}. This is a consequence of the use of the dark fringe for detection.

Figure 2 (body) shows three consecutive one-dimensional (1D) scans over a low concentration of terrylene molecules doped into a single crystal of p-terphenyl prepared by sublimation [14]. The sample stage is stepped by 1 micron in one transverse dimension every 5 s (30 ms lock-in time constant

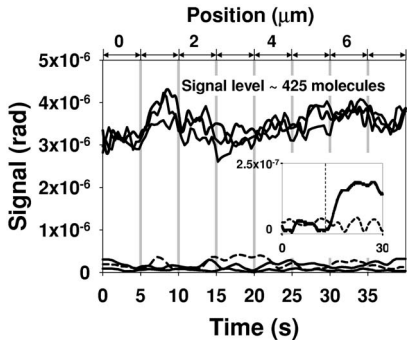

FIG. 2. Body: Scanning measurement of a low concentration terrylene/*p*-terphenyl single-crystal sample (250 ± 50 molecules/μm^2), with a step of the position of the sample by 1 μm every 5 s. The upper lines represent three one-dimensional scans over the same region of the sample. The two lower solid curves show the detected signal with red beam and green beam separately blocked, while the dashed line shows the signal for an undoped sample. Inset: Measurement of $11+-2$ molecules/μm^2 sample with the green beam unblocked at 13 s, along with the signal from an undoped sample. See text for details.

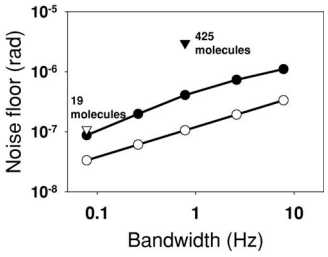

FIG. 3. Noise floor measured with undoped *p*-terphenyl crystal (upper line, filled circles) and theoretically predicted noise floor (lower line, open circles). Triangles represent measurements of the average phase-shift signal from samples containing ~425 molecules (solid triangle) and ~19 molecules (open triangle) in the laser spot, measured at the bandwidths indicated.

with an 11-point running average for an effective averaging time of 300 ms). The average green pump power of 38 mW (with spot size 2.5 μm^2 at the sample) ensured that the pump fluence of 18 mJ/cm^2 was above the calculated two-level saturation fluence of 4.7 mJ/cm^2 while still avoiding sample damage. Also shown in the bottom part of the figure are the noise floor (2nd lowest solid trace, signal with green laser blocked) and electronic noise floor (lowest solid trace, red laser blocked) with 300 ms lock-in time constant followed by an 11-point running average giving 3 s averaging time to show the traces more clearly. The signal level from a blank sample (an undoped sublimed *p*-terphenyl crystal) is also shown (dashed trace). These important controls confirm that the signals in the upper traces arise from terrylene molecules.

The *y* axis in Fig. 2 represents the detected photocurrent converted into equivalent radians of a differential phase shift, calibrated using an electro-optic modulator (EOM) located at the mirror-image position to the sample in the interferometer. According to our KK estimate [30], the phase shift per molecule at 633 nm is 2.4×10^{-9} rad assuming 1.7 μm^2 spot size, thus 3×10^{-6} rad average signal correspond to an average of 1250 molecules absorbing at any one position of the sample.

In addition to the KK calibration, a direct, independent estimation of the terrylene concentration was performed using single-molecule counting in a conventional single-molecule fluorescence microscope. First of all, these experiments use very thin sublimed samples (~3.5 μm thick), and when the focal plane is shifted, fluorescence signals are only observed from the central region of the sample over an axial distance roughly equal to the depth of focus of the microscope objective. (The absence of molecules from the surface regions is likely due to photooxidation.) Thus the important region of the sample is effectively two dimensional. Using an areal region of a typical fluorescence image 1.1 μm $\times$1.1 μm in size (large enough to capture essentially all photons from a single molecule spot), we measured the total number of photons above background from a single molecule in a very low concentration sample. Then the areal concentration of a higher concentration sample is determined by (total fluorescence counts in 1 μm$\times$1 μm)/(number of fluorescence counts from a single molecule). The nominal areal concentration of the sample in Fig. 2 was determined to be 250 ± 50 molecules/μm^2 (~425 molecules in 1.7 μm^2 probe beam spot). The observed (and repeatable) position-dependent signal variation in the three scans in Fig. 2 is as large as ±15%, larger than ±5%, the value to be expected from $\sqrt{N}$ variations with 425 molecules in the sampling volume. We attribute this excess variation to inhomogeneity in concentration produced by the crystal-growth process. In all our measurements, the signal per molecule estimated from KK was smaller than expected from the fluorescence calibration roughly by a factor of 3. We attribute this discrepancy to approximations inherent in the measurements entering the KK calculation, and use the direct calibration from fluorescence henceforth.

Figure 2, inset, shows a measurement completed on a lower-concentration crystal, 11 ± 2 molecules/μm^2 (within 1.7 μm^2 probe red beam spot, 19 ± 3 molecules) compared with a blank, undoped sample (dashed line). This trace was taken at one spot of the sample without scanning, because line scans in this ultralow signal regime were plagued by ~30% temporal fluctuations of the signal, a technical noise of unknown source. The green pump beam was blocked at first and opened at 13 seconds. The bandwidth was 0.078 Hz (equivalent to 1 s lock-in time constant). Similar signals showing clear detection of terrylene molecules were observed at other positions of this sample, but the expected $\sqrt{N}$ fluctutations could not be reliably observed in the presence of the technical noise.

For the purpose of both confirming the validity of the signal and measuring the actual noise floor, an undoped *p*-terphenyl crystal flake was measured with the result shown in Fig. 3, filled circles. This blank sample did not give any spurious signal above the noise floor down to 0.078 Hz bandwidth (solid circles), providing a determination of 4.0×10^{-7} rad/$\sqrt{\text{Hz}}$ as the limit of this measurement. This is a notable technological advantage compared to FM spectroscopy, where attempts to narrow bandwidth can uncover the presence of spurious signals, such as residual amplitude modulation (RAM) (Ref. [31]) arising from the EOM, which

require additional measures to suppress. When the red probe laser was blocked, the noise floor was lowered by ~5 dB, indicating that excess light noise from the local oscillator power and static dc level of the red probe laser ($P_{LO}+P_{dp}+P^{*}$) dominate the electronic noise. This level is 2 dB above the shot-noise limit calculated from the total power impinging on the detector. The lower line with open circles in Fig. 3 represents the theoretical shot-noise-limited minimum detectable phase shift given by Eq. (1) using parameters measured from the optical setup: $C=0.66$, effective probe power of $\eta_t P_{in}=2$ mW, $P_{LO}=0.1$ mW. This line corresponds to 1.2×10^{-7} rad/$\sqrt{\text{Hz}}$. Our measured noise floor (with blank sample) is about three times above the best-case theoretical noise floor. Triangles represent measurement points of the 250 ± 50 molecules/μm^2 sample (solid triangle) and 11 ± 2 molecules/μm^2 sample (open triangle).

The scaling of the noise floor of our Sagnac microscope agrees well with the theoretical expectation given by Eq. (1). With this in mind, we can project performance toward the ultimate goal, the detection of absorption and/or phase shift of a single molecule, if the problem of technical noise can be addressed. Under reasonable assumptions on spot size of the probe beam (1 μm) and bandwidth (0.1 Hz), and operating with half of the calculated saturation power of the terrylene molecule at 633 nm as the input probe laser power (8.9 mW), the saturation-limited minimum detectable phase shift is $\sim4.0\times10^{-9}$ rad, very close to the estimated phase shift from one terrylene molecule. It is remarkable that the actual system implemented is only one order of magnitude away from the ideal case.

In conclusion, this work has introduced and demonstrated a scheme for ultrasensitive scanning absorption measurements of a condensed matter sample suitable for room temperature operation. With a single-pass geometry in a light-noise-limited experiment, a sensitivity of 8.75×10^{-8} rad in 0.078 Hz bandwidth, and detection of signals arising from ~20 molecules at room temperature was achieved.

The authors thank M. D. Fayer for providing a mode locker, M. Digonnet for loan of the Nd:YAG laser, and the IBM Corporation for donation of electronic apparatus. This work was supported in part by the National Science Foundation, Grant Nos. 0241012 and 0237247.

[1] X. S. Xie and J. K. Trautman, Annu. Rev. Phys. Chem. **49**, 441 (1998).
[2] S. Nie and R. N. Zare, Annu. Rev. Biophys. Biomol. Struct. **26**, 565 (1997).
[3] M. Orrit and J. Bernard, Phys. Rev. Lett. **65**, 2716 (1990).
[4] T. Basche *et al.*, *Single Molecule Optical Detection, Imaging and Spectroscopy* (Verlag-Chemie, Weinheim, 1997).
[5] R. Y. Tsien and A. Waggoner, *Handbook of Biological Confocal Microscopy* (Plenum, New York, 1995).
[6] G. C. Bjorklund, Opt. Lett. **5**, 15 (1980).
[7] W. E. Moerner and L. Kador, Phys. Rev. Lett. **62**, 2535 (1989).
[8] A. O'Keefe and D. A. G. Deacon, Rev. Sci. Instrum. **59**, 2544 (1988).
[9] K. L. Bechtel *et al.*, Anal. Chem. **77**, 1177 (2005).
[10] G. A. Marcus and H. A. Schwettman, Appl. Opt. **41**, 5167 (2002).
[11] S. L. Logunov, Appl. Opt. **40**, 1570 (2001).
[12] I. M. P. Aarts *et al.*, Appl. Phys. Lett. **84**, 3079 (2004).
[13] A. Yariv, *Optical Electronics in Modern Communications* (Oxford University Press, New York, 1997).
[14] S. Kummer *et al.*, J. Chem. Phys. **107**, 7673 (1997).
[15] B. Lounis and W. E. Moerner, Nature (London) **407**, 491 (2000).
[16] J. Hwang, M. M. Fejer, and W. E. Moerner, Proc. SPIE **4962**, 110 (2003).
[17] G. Sagnac, C. R. Acad. Sci. III **95**, 1410 (1913).
[18] H. C. Lefevre, *The Fiber-Optic Gyroscope* (Artech House, Boston, 1993).
[19] P. A. Nicati and P. Robert, J. Phys. E **21**, 791 (1988).
[20] P. T. Beyersdorf, R. L. Byer, and M. M. Fejer, Class. Quantum Grav. **19**, 1585 (2002).
[21] D. Cotter *et al.*, Science **286**, 1523 (1999).
[22] N. J. Doran and D. Wood, Opt. Lett. **20**, 1424 (1995).
[23] M. Eiselt, Electron. Lett. **28**, 1505 (1992).
[24] J. P. Sokoloff *et al.*, IEEE Photon. Technol. Lett. **5**, 787 (1993).
[25] D. Jackson, Electron. Lett. **20**, 10 (1984).
[26] P. T. Beyersdorf, M. M. Fejer, and R. L. Byer, J. Opt. Soc. Am. B **16**, 1354 (1999).
[27] P. T. Beyersdorf, M. M. Fejer, and R. L. Byer, Opt. Lett. **24**, 1112 (1999).
[28] K. X. Sun *et al.*, Phys. Rev. Lett. **76**, 3053 (1996).
[29] K. X. Sun *et al.*, Opt. Lett. **22**, 1485 (1997).
[30] J. Hwang, M. M. Fejer, and W. E. Moerner (unpublished).
[31] E. A. Whittaker, M. Gehrtz, and G. C. Bjorklund, J. Opt. Soc. Am. B **2**, 1320 (1985).